PNNL-11783
UC-713

Direct Fast-Neutron Detection: A Status Report

A.J. Peurrung
R. R. Hansen
R. A. Craig
W. K. Hensley
C. W. Hubbard
P. E. Keller
P. L. Reeder
D. S. Sunberg

December 1997

Prepared for the U.S. Department of Energy
under Contract DE-AC06-76RLO 1830

Pacific Northwest National Laboratory
Richland, Washington

DISCLAIMER

Summary

This report describes the status of efforts to develop direct fast-neutron detection via proton recoil within plastic scintillator. Since recording proton recoil events is of little practical use without a means to discriminate effectively against gamma-ray interactions, the present effort is concentrated on demonstrating a method that distinguishes between pulse types. The proposed method exploits the different pulse shapes that are to be expected primarily on the basis of the slower speed of the recoiling fission neutrons. Should this effort ultimately prove successful, the resulting novel technology will have the potential to significantly lower cost and increase capability for a number of critical neutron-detection applications.

Considerable progress has been made toward a clear and compelling demonstration of this new technique. An exhaustive theoretical and numerical investigation of the method has been completed. We have been able to better understand the laboratory results and estimate the performance that could ultimately be achieved using the proposed technique. We have assessed the performance of a number of different algorithms for discriminating between neutron and gamma ray events. The results of this assessment will be critical when the construction of low-cost, field-portable neutron detectors becomes necessary. Finally, a laboratory effort to realize effective discrimination is well underway and has resulted in partial success.

Contents

Figures

Table

1.0 Introduction

Although proton recoil has been an accepted method for detecting fast neutrons since 1932 (Curie and Joloit 1932), it has failed to become a widespread, general method for neutron detection. This failure has persisted even though proton recoil within hydrogenous materials is both more rapid and more efficient than the moderate-and-capture process used in most common neutron detectors. The problem with proton recoil-based neutron detection is the inability to differentiate between proton recoil events and the much more common gamma-ray interactions. Unless this distinction can be made on an event-by-event basis, any neutron signal will be lost in a much larger background of gamma-ray events. The technique described in this report offers a method to discriminate effectively and efficiently between neutrons and gamma rays. Given the success of our discrimination method, development of a viable neutron detection technology will be straightforward. The resulting novel technology will have the potential to significantly lower cost and increase capability for a number of critical neutron detection applications.

Clearly, this effort depends on the fact that a significant and observable difference exists between the interaction physics of neutrons and gamma rays. There is ample reason to expect this to be the case. A 1-MeV neutron travels at roughly 5% of the speed of light and has approximately a 90% chance of recoiling at least once in passing through 10 cm of typical plastic scintillator. Subsequent interactions occur with an even higher probability and are separated by an average time of roughly 3 ns. Figure 1.1 shows six representative neutron pulses generated computationally according to a model described below. The neutron has a uniform probability for energy loss between 0% and 100% during proton-recoil interaction. Therefore, when recorded with a sufficiently fast electronic system, neutron pulses will exhibit a complex and random structure on a time scale of 10 ns or less. Gamma-ray pulses, in contrast, will exhibit far less structure because of the greater speed (30 cm/ns) of the photon. A 2-ns delay between repeated interactions of a single photon requires a total travel of at least 60-cm within the scintillator. This is unlikely to occur in any scintillator of modest physical size.

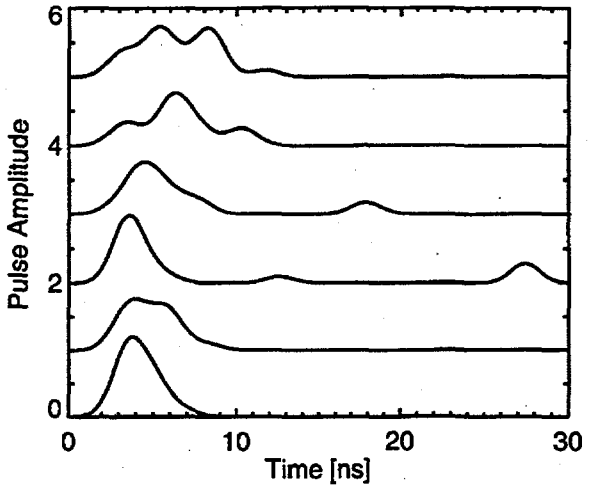

Figure 1.1. Six Numerically Calculated Neutron-Interaction Pulse Shapes. These six pulse shapes are typical and are calculated under the assumptions that fast but commercially available scintillators, PMTs, and data acquisition electronics are used.

The detection of neutrons for most current applications requires a moderator in conjunction with a medium that detects neutron capture by isotopes of helium, lithium, boron, or gadolinium. The technique described in this report, in contrast, directly records fast (fission) neutrons without the need for substantial moderation. The expected consequences of this fundamentally different approach are listed below:

1. Timing: The first 3 proton recoils of a fast neutron within plastic scintillator produce an average of 90% of the total light that can ever be observed. It should therefore be possible to localize fast-neutron detection in time to within 10 ns or less. In contrast, conventional moderate-and-capture neutron detection requires roughly 30 recoils and a total time of roughly 30 to 50 μs. We are confident, therefore, that direct fast-neutron detection (DFND) will offer time resolution that is 3.5 orders of magnitude more accurate than existing methods.

2. Efficiency: For modestly sized scintillators, DFND appears to offer significantly higher efficiency than conventional moderate-and-capture methods. This efficiency difference can be understood by considering the set of neutrons that undergoes 2 to 3 recoils, but is subsequently lost during the remainder of the moderation process and before capture can occur. Such neutrons may only be recorded via DFND. Although the relative efficiencies of the two methods for neutron depend on the details of a particular situation, theoretical and numerical analysis described below indicates that differences of 50 to 100% are typical.

3 Energy information: DFND retains a moderate degree of information about the energy spectrum of incident neutrons. Although the method may not be optimal for this purpose, it is quite likely that substantial spectral information can be acquired with little or no additional effort. In conventional moderate-and-capture neutron detection, of course, all energy information is lost during the moderation process.

4 Cost and complexity: Although complex hardware and electronics are not required for either neutron-detection method, there is reason to expect that DFND may ultimately be less expensive because there is no need for isotopically pure materials such as ^{3}He, ^{6}Li, or ^{10}B. Although the development costs for DFND may initially be significant, the corresponding replication costs should be quite reasonable. The dominant factor in the ultimate cost of DFND is expected to be the cost of photomultiplier tubes (PMTs).

A number of previous approaches to DFND have been explored (Knoll 1989, chap. 15), but none have found use in any but selected applications. These methods are either inefficient, or they fail to offer gamma-ray discrimination sufficient to measure weak neutron fluxes in predominantly gamma-ray backgrounds as required by many practical applications. Notably, DFND has been demonstrated in liquid scintillators based on the principle that pulse shape depends somewhat on charge-to-mass ratio (Hentley et al. 1988; Moszynski et al. 1992; Kunze et al. 1995). However, this method does not provide sufficiently effective discrimination between gamma rays and neutrons at fission energies (0.5 to 2.0 MeV). An additional drawback to this method is that pulse identities can be corrupted due to pileup under high-rate conditions.

DFND should significantly extend the capabilities of a number of non-destructive assay and non-destructive evaluation systems across the spectrum of possible applications. The timing information provided by DFND may allow the explicit determination of the location of a fission event, the energy of a detected neutron, and possibly even the cause of the fission event (spontaneous or induced). A primary challenge with active counting systems is to reduce the sensitivity of the neutron counters to neutrons from the interrogating neutron source. DFND greatly alleviates this problem when a low-energy americium-lithium (AmLi) interrogation source is used since only a few of these neutrons have energy

sufficient to permit detection. Coincidence counting applications in general will benefit from the 3.5 order-of-magnitude reduction in the accidental coincident background that results from faster event timing. Finally, many neutron detection systems are highly sensitive to the nature of the matrix material surrounding a neutron source. Such a matrix may moderate or absorb neutrons in a way that is not anticipated by the counting system. DFND should exhibit minimal matrix sensitivity since fast neutrons are the least affected by the exact quantity and nature of the source matrix.

We now anticipate three general areas of application for DFND technology:

1. Coincidence counting -- The anticipated characteristics of DFND systems should be especially well suited for coincidence counting in general and active coincidence counting in particular. These properties include precise event timing, blindness to AmLi neutrons, and matrix insensitivity.

2. Wide-area neutron-detection systems – The use of neutron counters for SNM detection over a large area is often limited by cost. Should DFND eventually provide low-cost, efficient neutron detection, it may find use for such applications.

3. Directional neutron detection – It may be possible to construct a directional neutron detector using DFND technology. The directional counting of fast neutrons should provide superior performance compared to currently available directional thermal neutron counters. Fast neutrons are generally more abundant and come directly from the fission source. Fast neutrons are also able to travel long distances through air without scattering.

2.0 Basic Principles

This section describes the results of theoretical and computational analyses intended to clarify the physics of neutron interaction within plastic scintillator. Many of these are derived from statistical analysis of thousands of individual neutron trajectories. Detailed information, such as the recoil times and positions and the energy losses, were obtained using the well-benchmarked code, MCNP (Briesmeister 1993). The model analyzed included the following assumptions:

- *Carbon:* The density and the composition of a typical plastic scintillator are correctly modeled for the purposes of neutron-transport calculations. As a simplifying assumption, however, carbon recoil is neglected in the data analysis. (Neutron energy loss via carbon recoil, however, is correctly accounted for.) Carbon-recoil events are simply not tallied as collisions. This assumption is based on the observation that carbon nuclei generate roughly one seventh as much as light per unit energy as recoil protons[1] and receive, on average, about a quarter of the recoil energy.
- *Geometry:* The scintillators in these calculations are assumed to consist of a planar slab with lateral dimensions large enough to be considered infinite. While this is certainly not a realistic assumption for all situations, it was chosen to simplify the interpretation of data and to simplify comparison of the results with existing neutron-detection technologies.
- *Incident Direction:* Neutrons are always assumed to be normally incident upon the scintillator. This assumption is appropriate for many problems and less appropriate for others, but serves to simplify the interpretation of data.

Figure 2.1 shows the frequency of energy loss as a function of energy loss for neutrons with an initial energy of 1.0 MeV. No reason exists to expect appropriately scaled results for other energies to be qualitatively different. The energy lost in all first collisions is equally distributed with respect to energy loss between 0.0 and 1.0 MeV, except for the effect of carbon recoils. Examining the histogram for only those first collisions that are followed by a second collision indicates a subtle difference between neutrons that undergo forward scattering and those that undergo back-scattering collisions as their first event. Those neutrons that undergo forward scattering lose little energy and continue in a direction generally toward the back side of the scintillator; the probability is large that these will be lost before undergoing a second collision. Those neutrons that undergo backward scattering lose most of their energy as they reverse direction and return toward the front of the scintillator. The significantly reduced mean free path between recoils for these neutrons nearly ensures that they will undergo subsequent recoil collisions. Note that although the second and third collisions are increasingly weighted toward lower recoil energies, as expected, it is possible that the second or third collision will be more energetic than the first. A simple probabilistic calculation of neutron interaction in pure hydrogen yields the result that the second proton recoil will exceed the first in energy roughly 31% of the time! The top two pulse shapes shown in Figure 1.1 are examples of this event.

[1] Bicron Corporation, product catalog. 1990. Data indicate that a typical plastic scintillator generates light with decreasing efficiency when excited by a gamma-ray interaction, proton recoil, and carbon recoil, respectively.

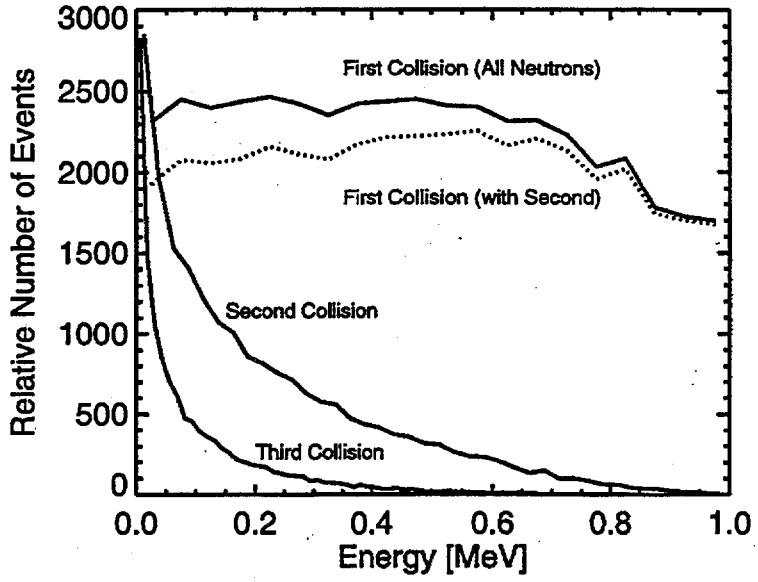

Figure 2.1. Histogram of the Distribution of Neutron-Recoil Energy Loss for Four Different Sets of Neutron Recoil Events Arising During the Interaction of 50,000 Neutrons. The sets are comprised of all first collisions, all second collisions, all third collisions, and those first collisions that are followed by a second collision. The second and third collision curves are vertically scaled to fit the plot, but the two sets of first collision data can be quantitatively compared.

It is important to know the exact timing of proton recoil to understand the general characteristics of neutron-interaction pulses. Figure 2.2 shows how the first three proton recoils are distributed with respect to time interval. These results were calculated assuming that neutrons strike a 10-cm-thick slab of typical plastic scintillator. It should be noted, however, that the proton-recoil timing depends somewhat on material choice, neutron energy, and assumed geometry. Pulses are more rapid in liquid scintillator than plastic scintillator since the former has greater net hydrogen content. Although the recoil interval does depend on the initial neutron energy, this dependence is weak as shown in Figure 2.3. Note that the average time interval in plastic scintillator is no less than 3 ns and has a minimum value for neutron energy of roughly 0.5 MeV. This insensitivity of average time interval to neutron energy arises because the neutron cross-section is roughly proportional to 1/v over this energy range (Marion and Young 1968). This means that information on the energy of the incident neutron will have to come from other data, such as the total pulse height. The dependence of recoil timing on scintillator size and shape arises from the fact that large time intervals correspond to long recoil-to-recoil spacings that may be less likely in a compact scintillator. It is significant, therefore, that small scintillators may have more difficulty discriminating between gamma ray and neutron interactions (the subject of the next section).

The above analysis indicates that any electronic system capable of distinguishing between gamma ray and neutron interactions in plastic scintillator must have at least 1-ns resolution. The bulk of the useful information in a neutron-interaction pulse is likely to occur between 3 ns and 10 ns after the start of the pulse. This is the interval during which observable neutron recoils may still be occurring, yet any gamma-ray interaction is complete.

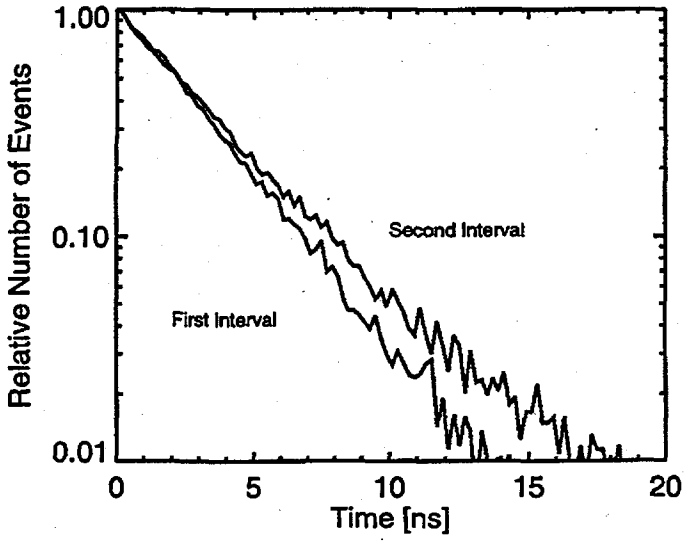

Figure 2.2. Histogram Showing the Distribution of Time Intervals Between the First and Second Recoils and Between the Second and Third Recoils

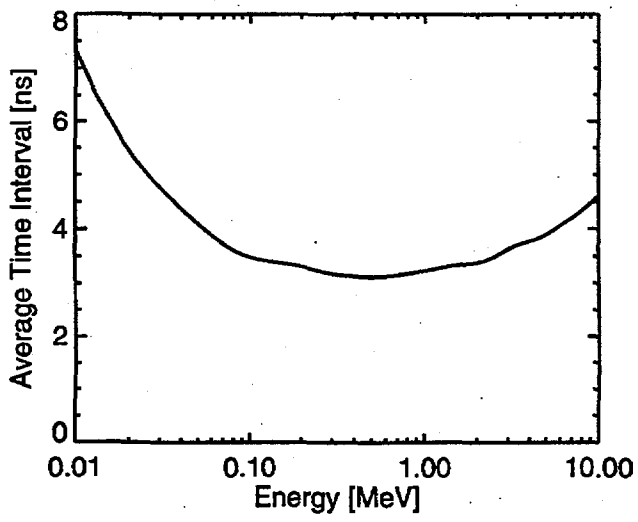

Figure 2.3. Plot Showing the Theoretically Expected Average Time Interval Between Hydrogen Recoils As a Function of Neutron Energy

It is useful to distinguish between the maximum theoretically possible efficiency and the actual expected efficiency for DFND in plastic scintillator. The theoretically possible efficiency is defined here as the fraction of incident neutrons that undergoes two or more hydrogen recoils within the plastic scintillator. Clearly, not all of the interactions that meet this criterion are sufficiently distinct from gamma-ray interactions that they can unambiguously be labeled as neutrons. However, this measure is a useful benchmark for discussion because any neutron that does not recoil at least twice will *always* fail to be correctly identified and thus will not be detected. The theoretically possible efficiency is independent of parameters such as the exact discrimination algorithm, light-collection efficiency, scintillator size, scintillator decay time, and PMT characteristics. It does depend strongly on the neutron-energy spectrum and on the scintillator geometry.

Figure 2.4 shows the number of neutrons remaining as a function of the number of hydrogen collisions within various thicknesses and composition of hydrogenous material. The results are shown for four different thicknesses and three different hydrogenous materials of 10.16-cm (4-inch) thickness. A number of interesting conclusions can be drawn from these data. The theoretical maximum efficiency for 2.54-, 5.08-, 10.16-, and 20.32-cm-thick (1-, 2-, 4-, and 8-inch-thick) scintillators is 27%, 55%, 82%, and 90%, respectively. These results indicate that very little reason exists to design neutron detectors thicker than 10.16 cm using this technology. It is also clear that a liquid scintillator would have a greater theoretical efficiency than a solid scintillator of the same size and shape. (However, the increased hydrogen density reduces the recoil timing intervals and may make it more difficult to correctly identify neutron interactions.) Figure 2.4 also clearly demonstrates that a substantial fraction of the incident neutron population is detectable via the method proposed here, but would leave the scintillator before they could be captured at thermal energies. Because this is especially true for thin (2.54-cm) scintillators, we expect the relative advantage of the present method to be greatest for thin scintillators.

Analyzing the proposed method of neutron detection requires careful Monte Carlo modeling, not only of the neutron-interaction physics, but also of the generation, collection, and recording of scintillation photons. The neutron-interaction physics was modeled using the MCNP neutron transport

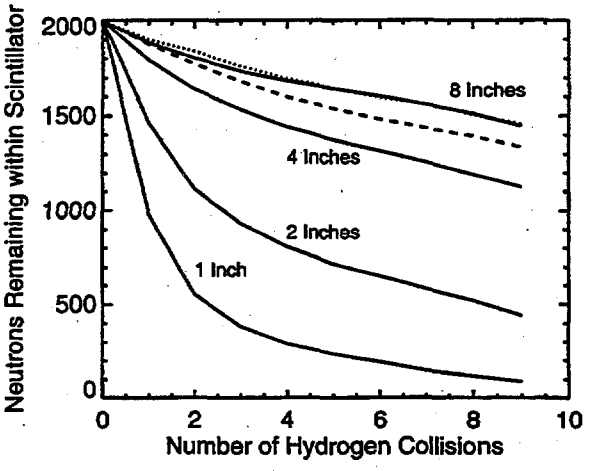

Figure 2.4. Number of Neutrons Remaining Within a Slab of Scintillator as a Function of the Number of Hydrogen Collisions that Have Taken Place. The four solid lines assume that typical plastic scintillating slabs with thicknesses of 2.54, 5.08, 10.16, and 20.32 cm (1, 2, 4, and 8 inches) are used. The dashed and dotted curves assume a 10.16-cm (4-inch) slab of material with the density and composition of typical liquid scintillator and polyethylene, respectively. Polyethylene does not scintillate, but is included for comparison.

code as described in the preceding section. For each energy deposition in the scintillator, a separate Monte Carlo algorithm was invoked to properly randomize the quantity and emission times of the resulting discrete photons. Once emitted, each photon was assigned a random travel time intended to approximate the effect of finite scintillator size on the photon-collection process. Typically, 0.5 ns was used for the "spread" in these random travel times because this is the time an optical photon requires to travel approximately 10 cm. Although this "optical" model is crude, it was found to have a minor effect on the predicted detection efficiencies. The choices as to which scintillation photons reach the PMTs and which photons result in photoelectron emission within the tubes was again made by a randomizing Monte Carlo algorithm. The final output pulse was composed of the sum of individual photoelectron pulses, each of which was assumed to mimic the output of a typical, high-speed, 5.08-cm diameter PMT.

The pulse-simulation model described above serves a dual purpose in our effort to develop DFND technology. First, when used to generate pulses corresponding to both neutron and gamma ray interactions, it allows testing and optimization of computational algorithms intended to discriminate between the two types of pulses. (This is the subject of the next section.) For this purpose, a second set of pulses corresponding to gamma-ray interactions was also generated, under the assumption that the gamma ray deposits between 0 MeV and 1 MeV of proton-equivalent energy within 1 ns. This is described below. Second, this model can be used as a tool for understanding the characteristics of actual laboratory pulses.

The model for gamma-ray interactions assumed above, while crude, is experimentally reasonable. A 1.0-MeV gamma ray traveling in plastic scintillator has a mean free path of roughly 13-cm. Since it covers this distance in roughly 0.45 ns, gamma-ray interactions should be significantly more rapid than neutron interactions. It should be nearly impossible for a gamma ray to travel for more than 1 ns within a scintillator of limited size. Like neutrons, scattered gamma rays of lower energy and therefore with a higher interaction cross section may be produced by the initial interaction. Because, however, gamma rays of all energies travel at the same speed, subsequent interactions are likely to occur at faster and faster rates.

In some environments, an energy threshold may be required to discriminate against the pair-production mode of gamma-ray interaction. A positron produced by a pair-production event may not annihilate for 2 to 5 ns (West 1973). The aggregate pulse produced by the initial pair production and the subsequent interactions of 511 keV gamma rays may have a shape that would be classified as a neutron event by any discrimination algorithm. However, pair-production cross-sections in plastic scintillator are small for photon energies less than 3.0 MeV. (The mass attenuation coefficient for pair production in water at 3.0 MeV is roughly 10^{-3} cm^2/g.) Although photon fluxes above this energy are small, this interaction can be discriminated against, if necessary, using an energy threshold. A 3.0-MeV pair-production event must deposit roughly 2.0 MeV of energy via the electron and positron. Since a neutron with energy in excess of 5.0 MeV would be necessary for such an interaction,[1] an upper-energy threshold would eliminate pair-production events without much loss of neutron efficiency from a fission neutron source.

[1] Bicron Corporation, product catalog. 1990. Data indicate that a typical plastic scintillator generates light with decreasing efficiency when excited by a gamma-ray interaction, proton recoil, and carbon recoil, respectively.

3.0 Discrimination and Expected Efficiency

This section evaluates a number of different algorithms to understand which algorithms are able to efficiently record neutron events while effectively rejecting gamma-ray events. Each of the seven algorithms discussed below derives a single, scalar parameter from a particular pulse. This parameter could be used to discriminate between neutrons and gamma rays in much the same way that pulse height is used to differentiate event types in many other radiation detection systems. However, algorithm-based discrimination has the advantage that the discrimination threshold itself can be made a function of pulse height. In this way, the threshold can be made more "stringent" for low amplitude pulses with poor statistics and more "lenient" for large-amplitude pulses with superior statistics. The procedure was used for several of the algorithms described below. Examples of this procedure for particular discrimination algorithms can be found in Figures 3.1 and 3.3.

To compare discrimination algorithms, two sets of pulses were computed to model the interactions of 2000 neutrons and 2000 gamma rays. These pulses were calculated as described above under the assumption that scintillator light was collected with 6% efficiency by PMTs with 20% quantum efficiency. Fission-spectrum neutrons are assumed to be normally incident upon a scintillating plane that is 10 cm thick.

Table 3.1 lists the seven algorithms studied, their optimal efficiency, and any comments germane to that algorithm. This model assumes a 10-cm-thick planar scintillator with normally incident fission spectrum neutrons. The light is assumed to be collected with 6% efficiency, and the PMTs are assumed to be 6% efficient.

Table 3.1. Listing of Seven Algorithms and their Optimal Efficiencies for a set of 2000 Numerically Simulated Neutron and Gamma Ray Pulses

Algorithm	Optimal Efficiency	Comments
Fit peak rise to Gaussian	17%	Little use expected
Fit peak decay to exponential	Very poor	Failed
Count number of peaks	8%	Little use expected
Early area fraction	49%	Easy to implement
Pulse width	54%	Good but complex
Neural net	56%	Best algorithm
Time cutoff	42%	Simple/useful for rough cut

As can be seen from Table 3.1, several algorithms offer acceptable performance. As will be discussed in Section 5.0, it may be desirable to use a simpler, hardware-implemented algorithm for "rough cut" discrimination followed by a more complex, but more precise, algorithm for the final determination of pulse identity. The early area fraction, neutral network, or time cutoff algorithms may be well suited as a "rough cut" algorithm. The neural net and pulse-width algorithms may be well suited as second-stage discriminators. Each of the algorithms is described in more detail below:

3.1 Fit Peak Rise to Gaussian

Description

For each event trace, a "best fit" Gaussian curve is found by fitting the region from the start of the trace to the first maximum using a three-parameter simplex fitting algorithm. The best-fit Gaussian is then compared to the actual trace and a chi-square error sum is computed as the discrimination parameter. The Gaussian amplitude, sigma, and centroid parameters are allowed to vary during the fit—i.e., A, B, and C in the equation

$$F = \frac{A}{B\sqrt{2\pi}} e^{-(t-C)^2/(2B^2)} \tag{3.1}$$

This is actually the first of the "fitting" algorithms tested on the DFND simulated data sets and also the first use of a simplex fitting algorithm. An advantage of the simplex method is that it is not particularly sensitive to the initial coordinates, but it is best to start off with values that are close to the final value.

Results

The fitting algorithm was applied to every trace in the simulated gamma-trace data set, and the corresponding chi-square errors were then sorted. A value equal to the second largest error was chosen as the magic peak discrimination error since, by definition, using this value would only misidentify one gamma out of the 2000 in the data set. When this same test was applied to the simulated neutron trace data set, only 17.3%of the neutrons were correctly identified.

3.2 Fit Peak Decay to Exponential

Description

The decay region following the first maximum of each event trace is fit to an exponential decay curve using a three-parameter simplex fitting algorithm. The parameters allowed to vary during the fit are amplitude, time constant, and constant offset—i.e., A, B, and C in the equation

$$F = Ae^{-(t/B)} + C \tag{3.2}$$

The best fit exponential is then compared to the actual trace, and a chi-square error sum is computed as the discrimination parameter.

A number of problems make this more complicated than the Gaussian fit algorithm. First, the pulses are not really very exponential-like on their decay sides. This means that fits are generally poor, and the exponential (which has a constant offset component) always drops below zero as it approaches its asymptote. This contributes significantly to the error sum since the real pulse data *never* drops below zero. Secondly, it is difficult to decide over what part of the pulse the fit should be done.

Results

The simplex fitting algorithm produces excellent results when the traces consist of nicely shaped single-peaked curves, but fails for traces with more structure on the decay side. Unfortunately, even the "nicest" of peaks is not particularly exponential-like in shape, and the "ugly" ones definitely are not! An exponential fit algorithm will likely not make a viable discrimination.

3.3 Count Number of Peaks

Description

This is a very simple algorithm that relies on the assumption that, in general, gamma ray peak traces have fewer maxima than neutron traces. The number of peak maxima are counted for each pulse in the simulated gamma ray data set, and the largest number of maxima found for a single trace, M, is used as a pulse-type discriminator. Traces from the simulated neutron data set that have more than M maxima are counted as neutrons, and those with fewer are counted as gamma rays.

Results

Unfortunately, the typical gamma trace is not as singularly peaked as we would like. With $M = 5$, four gamma rays out of 2000 were misidentified as neutrons (0.4%). With $M = 5$ applied to the neutron data set, only 271 of 1772 neutrons were correctly identified (15.3%). Increasing M to six yielded 0/2000 misidentified gamma rays, but only 141/1772 properly identified neutrons (8.0%).

3.4 Early Area Fraction

Description

The parameter used for this algorithm is simply the fraction of total pulse area occurring during the initial time τ (its "early area The idea behind this algorithm is simply the fact that gamma-ray events should be largely complete in a shorter time than neutron events.

For a particular value of the integration time, τ, the algorithm proceeds as follows: both the neutron and gamma ray pulses are placed in a two-dimensional phase space consisting of the early and total areas. A bounding curve is found that separates all but one of the gamma-ray pulses from the maximum number of neutron pulses. The number of neutron pulses that are correctly identified in this way is considered to be the algorithm efficiency.

Results

Figure 3.1 shows the phase space plot for an integration time of 8 ns. In all cases, it was found that a straight line could be used for the bounding threshold curve. To find the optimal integration time, this procedure was repeated for a whole range of integration times as shown in Figure 3.2. The maximum efficiency of 49% was found for an integration time of 8 ns.

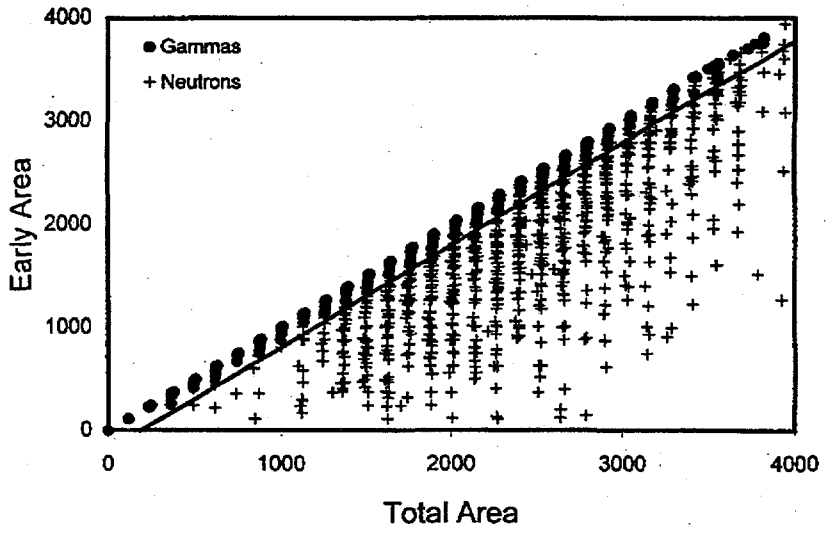

Figure 3.1. Plot of Early Area vs. Total Peak Area for Numerically Generated Sets of 2000 Neutron Pulses and 2000 Gamma Ray Pulses. The line represents the bounding curve that most effectively separates the neutron and gamma ray pulses. The cutoff time for this example is 8.0 ns.

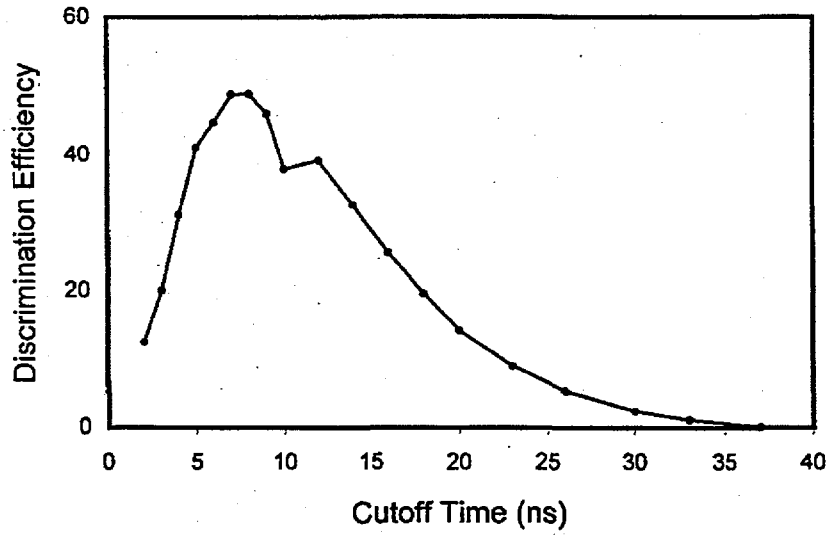

Figure 3.2. Graph Showing the Algorithmic Efficiency of the "Early Area" Method as a Function of the Cutoff Time Used. The optimum cutoff time is found to be 8.0 ns.

3.5 Pulse Width

Description

For each pulse trace, a width is calculated according to the formula

$$\text{width} = \int |t - T|^n \cdot f(t)dt \qquad T = \frac{\int t \cdot f(t)dt}{\int f(t)dt} \tag{3.3}$$

where *f(t)* represents the pulse trace, *t* is time along the trace axis, *n* is some constant greater than zero, and *T* is the weighted mean time of the pulse (a sort of time centroid). The exponent *n* is varied to find the optimal form of the algorithm. The pulse width calculated in this way is used as the discrimination threshold. The threshold is again treated as a function of total pulse area. The idea behind this algorithm is that gamma ray pulses should be narrower than neutron pulses.

Results

Figure 3.3 shows all of the neutron and gamma ray pulses located in the width/area phase space for a value of n = 1.4. In every case, it was found that an exponential curve of the form

$$Y = Ae^{-(x/B)} + C \tag{3.4}$$

was able to effectively separate the neutron and gamma-ray pulses, where *A* and *B* are constants chosen to optimize the separation, *x* represents the pulse area, and *Y* represents the pulse width. Figure 3.4 shows the efficiency that was obtained as a function of the parameter n. The optimal efficiency of 54% was obtained for a value of 1.4 for the exponent n.

3.6 Neural Net

Description

In this study, neural networks and traditional pattern recognition techniques were trained to discriminate between neutron events and non-neutron events. The outputs of these classifiers were thresholded to produce binary discriminators with thresholds set by the stipulation that a non-neutron event misclassified as a neutron event can not be tolerated. The Pattern Recognition Workbench software from Unica (*Pattern Recognition Workbench 2.1*, Unica Technologies Inc., Brighton, Massachusetts, 1997) was used in this study. The neural network pattern classifiers implemented were a simple linear perceptron, the standard backpropagation-trained multilayer perceptron (MLP), and radial basis function (RBF) network. The traditional pattern classifiers implemented were a k-nearest-neighbors (kNN) classifier and a linear regression (LR) classifier. The pulses were normalized to unit mean and variance (i.e., zero-score). Each discrimination technique was trained with a 4-fold cross validation technique where 75% of the data were used to train the event detector, and 25% were used to test the technique during each of the four runs. The pattern classifiers tested in this study produce an analog output on a scale of 0 to 1 to represent whether the event is a neutron event. By thresholding the output, a binary decision is made with all events above the threshold classified as neutron events. The choice of the threshold is varied to fit the desired selectivity and sensitivity.

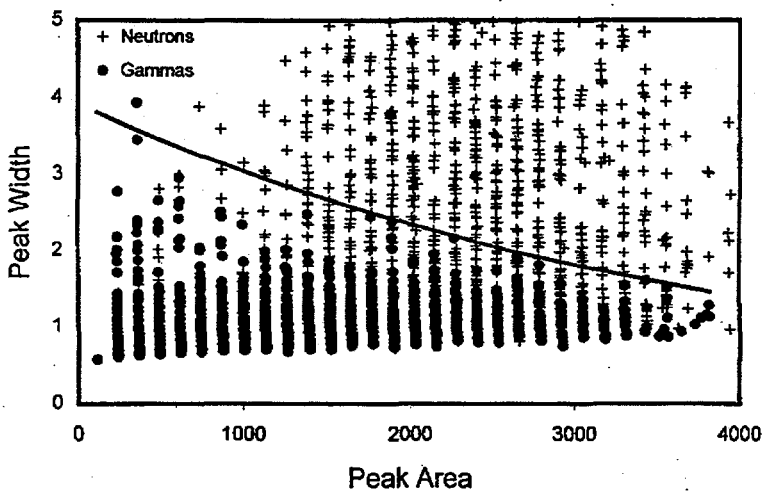

Figure 3.3. Plot of the Pulse Width vs. Pulse Area for Numerically Generated Sets of 2000 Neutron and 2000 Gamma Ray Pulses. The line represents the bounding curve that most effectively separates the neutron and gamma ray pulses. The exponent used for the width calculation was 1.4.

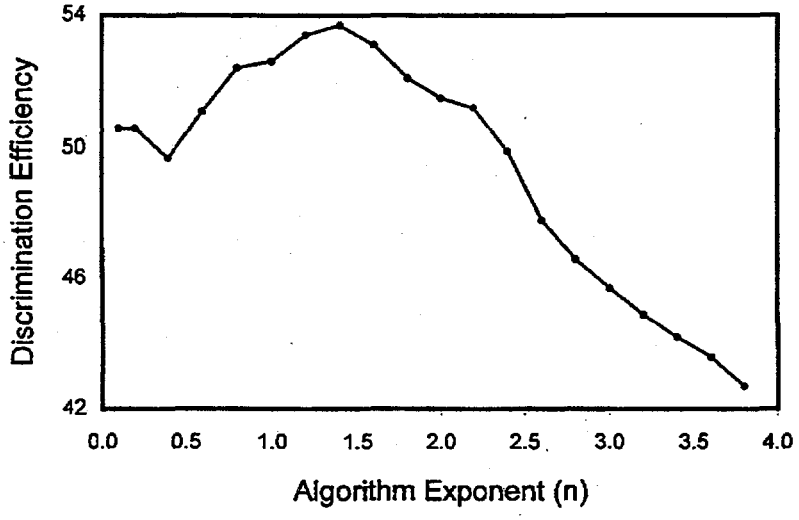

Figure 3.4. Graph Showing the Algorithmic Efficiency of the "Pulse Width" Method as a Function of the Exponent Used for Calculation of the Pulse Width. The optimum exponent was found to be 1.4.

Results

The results show that a neutron-event discriminator can be developed by using multilayer perceptron neural networks, radial basis function neural networks, and linear regression for at least simulated data. Both the kNN and the simple linear perceptron were not able to fully reject gamma events misclassified as neutron events. In the best case, one gamma ray was misclassified at the same time that 56% of all neutron events were correctly recognized. Other multilayer perceptron neural networks achieved zero false positives, but with lower neutron identification rates. The RBF neural network and LR discriminators also achieved zero false positives, but at low neutron detection rates. If these simulated data accurately model the complexities of real data, then the backpropagation MLP neural network will likely provide adequate discrimination capability for the neutron-event discriminator and is probably the best choice of the neural net techniques tried in this study.

3.7 Time Cutoff

Description

This is a vastly simplified form of the early area fraction algorithm that compared trace integrals before and after a particular time value. This algorithm simply integrates the trace beyond a cutoff time and checks for an effectively non-zero result. The idea is that, in general, gamma events will be over sooner than neutron events, so some time, t_c, should exist beyond which all gamma events will be completed.

Results

A value of 13.6 ns was determined for t_c by examining each trace in the simulated gamma-ray-pulse data set. This value was chosen to ensure that only one gamma ray is misidentified. Using this value as the cutoff time described above, integrals were calculated for each trace in the simulated neutron data set. Any pulses that yielded non-zero integrals were considered to be neutrons. This algorithm correctly identified 42.4% of the neutrons. While this is somewhat less efficient than other algorithms, this technique is clearly the simplest and fastest of the well performing algorithms. This algorithm would be easy to implement in hardware and could serve either as the only discrimination algorithm or, by decreasing the value of t_c slightly, it would make a good "rough cut" algorithm.

4.0 Experimental Progress

The continuing goal of our experimental effort is to clearly demonstrate that algorithmic discrimination between neutron and gamma ray interactions in plastic scintillator is feasible and effective. Subsequent goals will be to optimize the efficiency, maximize the gamma-ray rejection, and confirm various aspects of the theoretical and computational model described above.

This section is organized as a list of the tests that have been performed and their results and implications. The first and most important test, of course, is an attempt to differentiate between neutron and gamma ray pulses. As will be described below, this test was only partially successful due to the unanticipated structure and breadth of the gamma ray pulses. A number of subsequent tests were completed to understand the causes (and cures) for this behavior.

4.1 Neutron/Gamma Ray Differentiation Test

To complete this test, it was necessary to set up a time-of-flight measurement system as shown in Figure 4.1 so that the identity of particles interacting within the scintillator would be known. This arrangement relies on the fact that neutrons and gamma rays can be easily distinguished by the time required to travel from the "trigger" scintillator to the "experimental" scintillator. A coincidence between the two scintillators, which were normally separated by 15-cm, was required for each of the events described below. Under these conditions the gamma ray flight time is 0.5 ns, while the neutron travel time is roughly 10 ns. An example of a combined time-of-flight and pulse-height spectrum is shown in Figure 4.2. Note that there is ample separation between the set of gamma ray and the set of neutron pulses. Note also that, as expected, the higher amplitude neutron pulses occur for those neutrons that arrive more quickly. On the basis of these data, we conclude that time-of-flight can be used as an effective means of learning the identity of particles interacting in the scintillator under study.

The time-of-flight system described above allows careful, statistical comparisons to be made between sets of neutron pulses and sets of gamma-ray pulses. Figure 4.3 shows "width spectra" for 100 gamma ray and 100 neutron pulses. The Bicron type 418 scintillator used for these data consisted of a 5-cm-diameter, 7.5-cm-long cylinder oriented with its axis pointed at the ^{252}Cf fission source. Because this scintillator has rather small lateral dimensions, the fraction of interacting neutrons that would be expected to undergo multiple recoils is relatively small, possibly on the order of 10%. This educated guess is supported by the data in Figure 4.3, which indicate that the widest 10 to 20% of neutron pulses are significantly wider than the widest 10 to 20% of gamma-ray pulses. Thus, this test confirms the validity of our fundamental approach to DFND by illustrating that the physics of neutron recoil does significantly affect the observed pulse shapes.

Figure 4.4 shows all 100 of the gamma ray pulses used for this test, illustrating the reason why this test can only be considered a partial success. Much "structure" appears in the tailing sides of many of these pulses, resulting in unacceptable increases in the pulse width and making pulse-by-pulse discrimination between neutrons and gamma rays next to impossible.

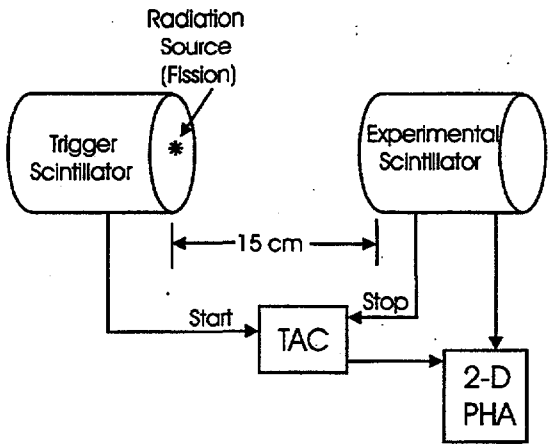

Figure 4.1. Schematic Drawing Showing the Time-of-Flight Technique Used To Label Pulses As Neutron or Gamma Ray Pulses Before Interaction in the Scintillator. This method allows assessment of the performance of a direct fast-neutron detector.

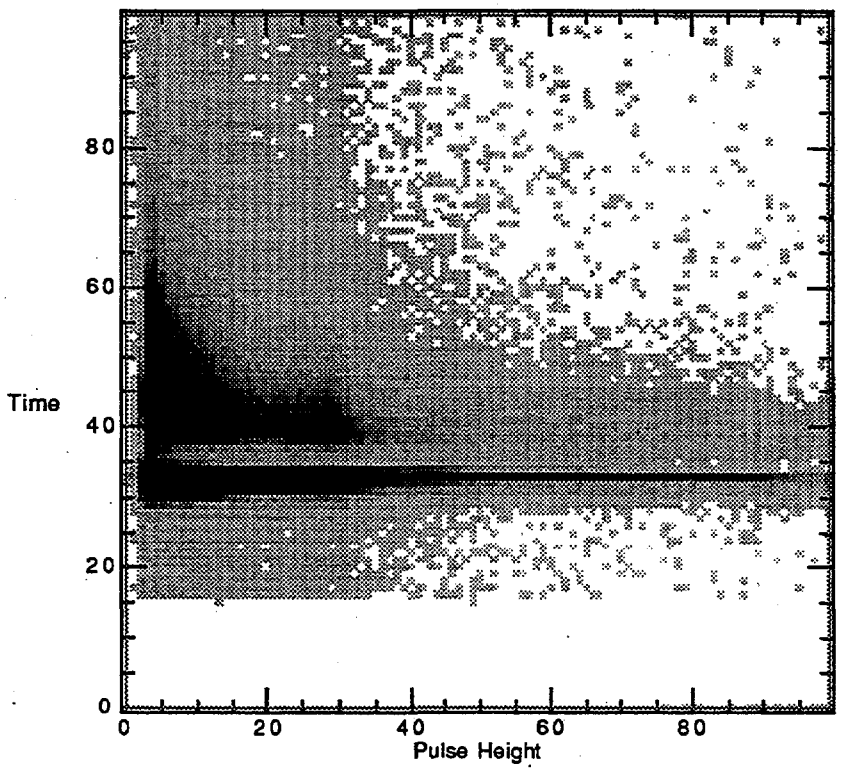

Figure 4.2. Combined Time-of-Flight and Pulse Height Spectra. This plot further illustrates the pulse labeling method. Each time channel represents 0.88 ns.

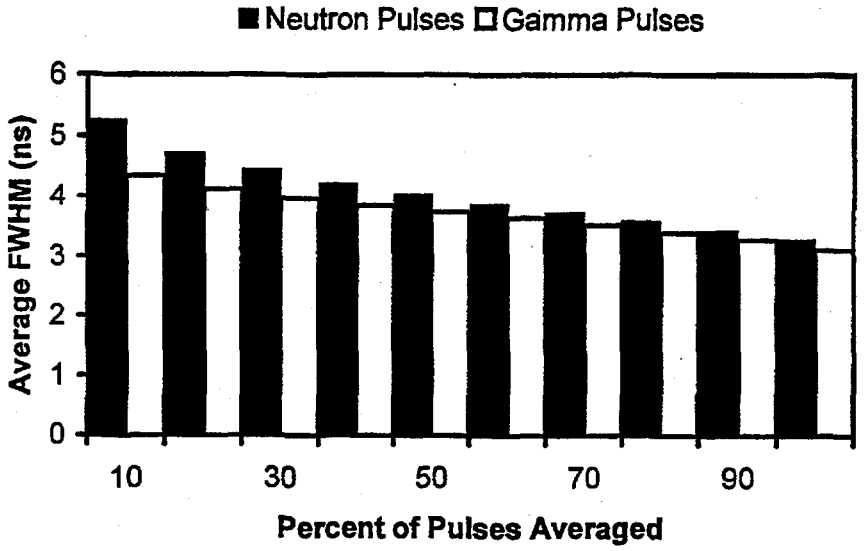

Figure 4.3. Plot comparing the averaged width of various subsets of Experimentally Acquired Sets of 100 Neutron and 100 Gamma Ray Pulses. The pulses were sorted by width before selecting the fractional subsets. For example, the first data point shows the average width of the widest 10% of the neutron and gamma ray pulses.

Figure 4.4. Plot Showing 100 Experimentally Acquired Gamma Ray Pulses. The average width for this set is roughly 3.3 ns.

4.2 Cherenkov Test

To understand the sources of pulse structure and broadening, we used light pulses generated by Cherenkov radiation within ordinary lucite plastic to simulate the performance of a "perfect" scintillator. Cherenkov light pulses have a duration of significantly less than 0.1 ns because the light can only be emitted when the electron travels faster than the effective speed of light (for plastic). Any structure observed on Cherenkov pulses must result from some problem with the PMT or remainder of the electronic system. A set of 100 Cherenkov pulses and the associated width spectrum are shown in Figure 4.5. Clearly, these pulses are free of the structure that plagues both the neutron and gamma ray pulses generated within plastic scintillator. In fact, the width of these pulses is nearly what would be expected on the basis of the technical specifications for the PMT used in this experiment. (The PMTs used here were Hammamatsu model R2083.)

4.3 Energy Tests

Further clues to the nature of the observed pulses can be gained by investigating the dependence of the pulse characteristics on pulse height. The width spectra for pulse sets with a number of different energies are shown in Figure 4.6. The fact that the spread in pulse widths decreases with increasing total pulse height clearly indicates that the anomalous pulse "structure" is of a random, statistical nature. The average width of the pulses, however, is only weakly dependent on the pulse height. The random pulse structure should not be responsible for the excessively large widths.

4.4 Scintillator-Size Tests

Some have speculated that unwanted pulse structure arises from the optical travel time of light produced by the scintillator. For this and other reasons, the dependence of the pulse characteristics upon pulse shape was studied using scintillators alike in every way but size. Figure 4.7 shows the width spectrum for 0.64-cm- and 7.62-cm-thick scintillating cylinders that are 5.08 cm in diameter. There is only a minor difference between these two pulse sets that probably does arise from the differing optical travel times. However, this test indicates that optical effects are not the primary cause of the unwanted pulse structure.

4.5 Scintillator-Surface Tests

As an additional test of the importance of optical effects, pulse sets taken from scintillators with different surfaces were acquired and compared. Figure 4.8 shows the pulse width spectra for two scintillators with absorbing and diffusely reflecting surfaces, respectively. The minor differences between these sets probably do arise from optical differences (and possible random statistics). However, these data also fail to support the hypothesis that optical effects cause unwanted structure.

4.6 Radiation Type Tests

It has been speculated that the unwanted structure arises from some sort of unanticipated interaction physics. For example, a gamma ray might Compton scatter within the scintillator, exit the scintillator, Compton scatter again in the general environment, and finally re-enter the scintillator for a final interaction. In this way, a gamma-ray interaction might acquire a structure as a result of its protracted interaction. Additionally, it is possible that gamma-ray pulses might interact in the PMT itself, producing highly irregular pulses. While none of these explanations is particularly convincing, it is

prudent to compare pulse sets that are alike except for the type of radiation causing them. If these sets are very similar, then interaction physics can be generally dismissed as the cause of unwanted structure.

Figure 4.9 shows the pulse width spectra for two pulse sets produced by gamma ray and beta interactions, respectively. These sets are identical except for random statistical differences. Clearly, the problem does not involve interaction physics.

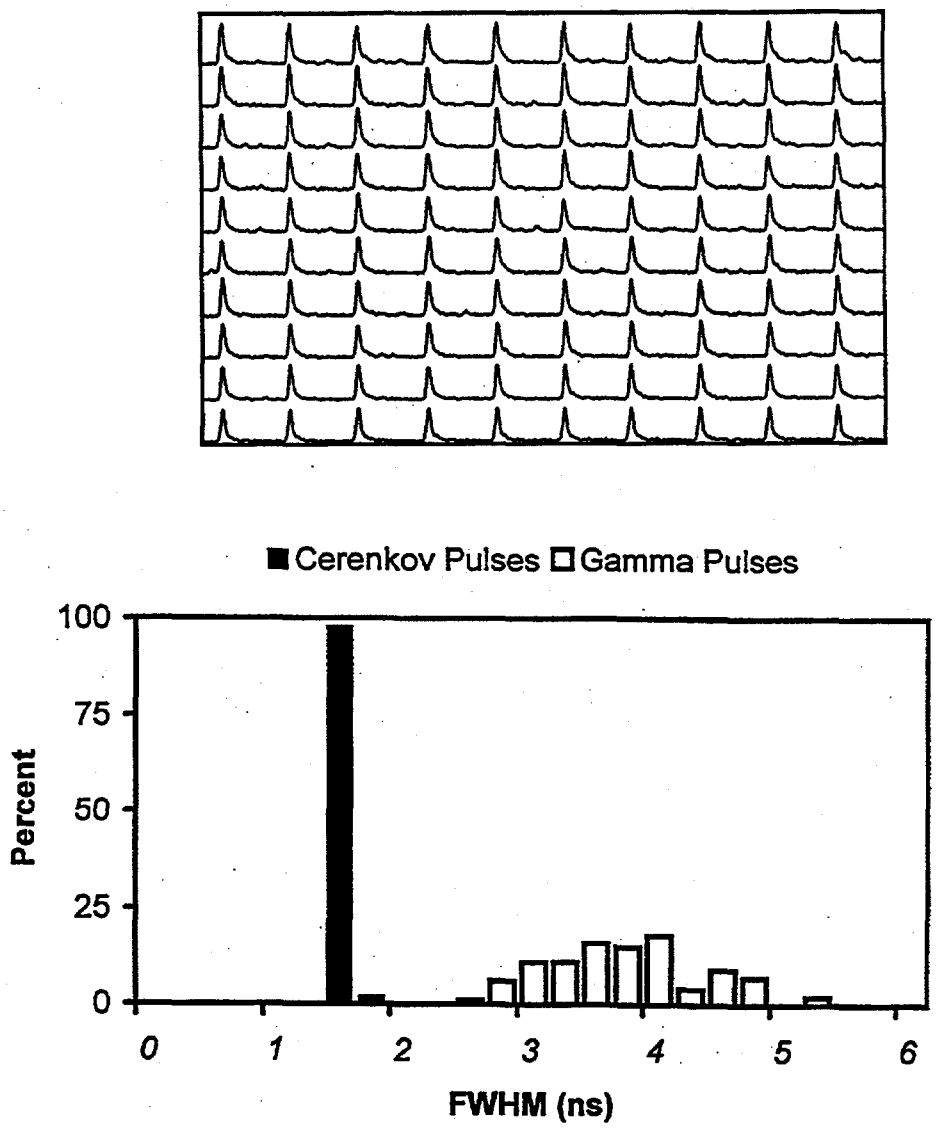

Figure 4.5. Plot Showing 100 Experimentally Acquired Cherenkov Pulses and the Associated Width Spectrum. The average width for this set is roughly 1.4 ns. The width spectrum for a typical set of gamma ray pulses is also shown.

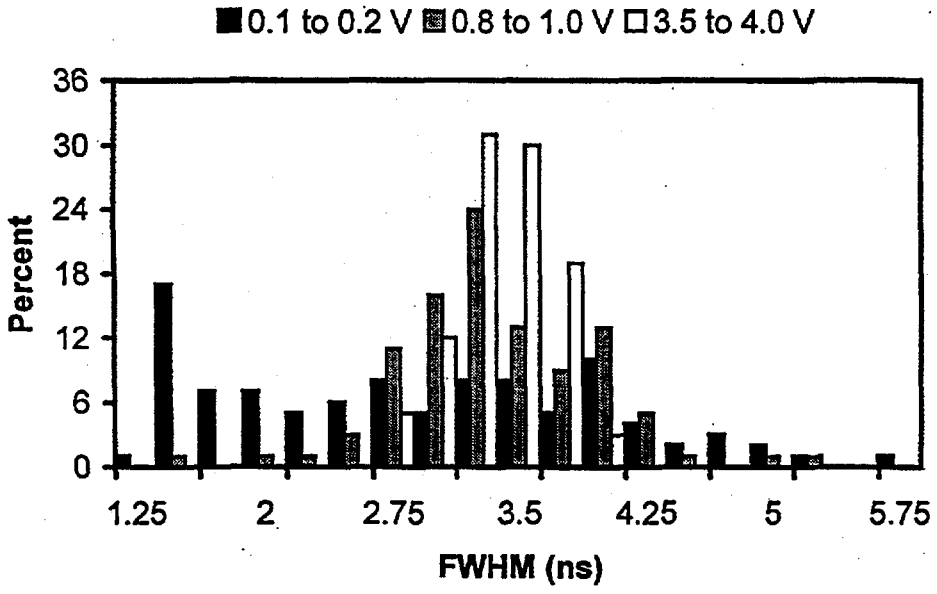

Figure 4.6. Plot Showing Width Spectra for Sets of Pulses with Different Pulse Heights

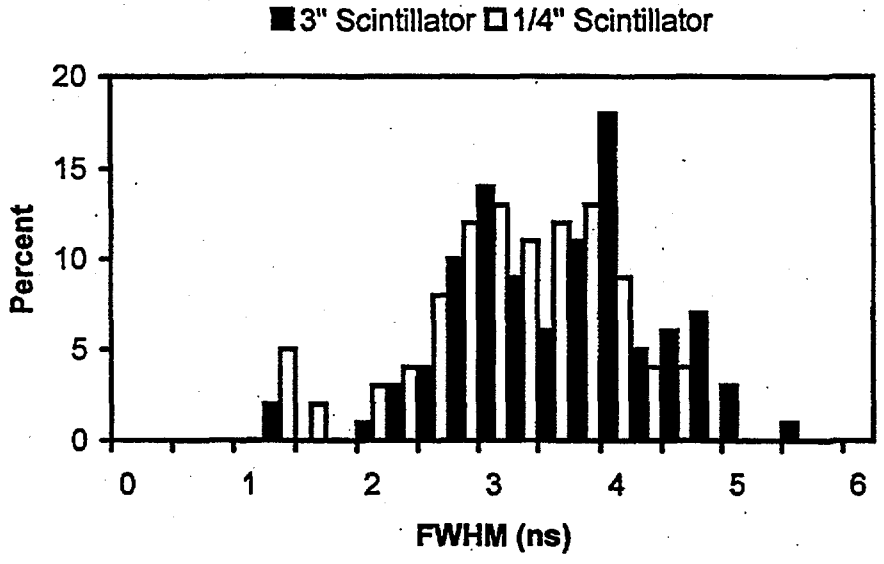

Figure 4.7. Plot Showing Width Spectra for Sets of Pulses Acquired Using Scintillators with Different Sizes

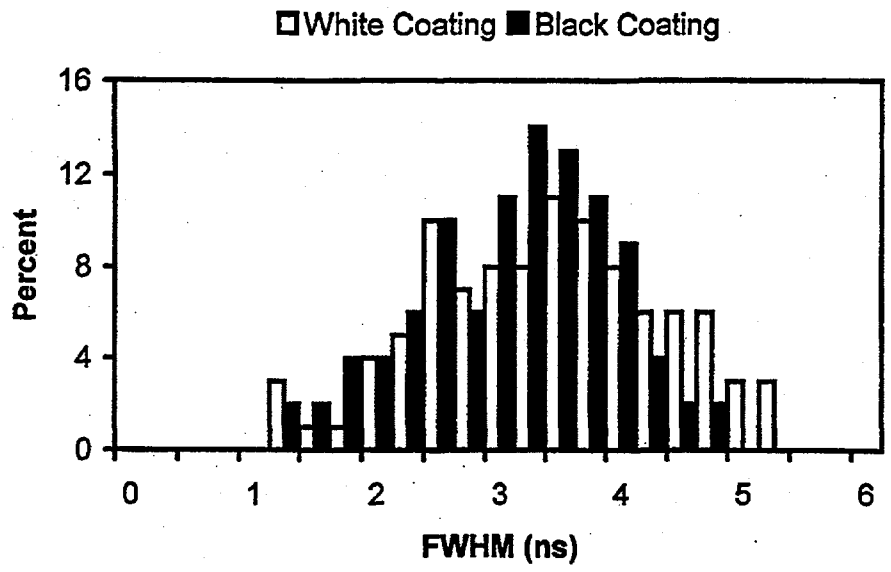

Figure 4.8. Plot Showing Width Spectra for Sets of Pulses Acquired Using Scintillators with Different Surface Characteristics

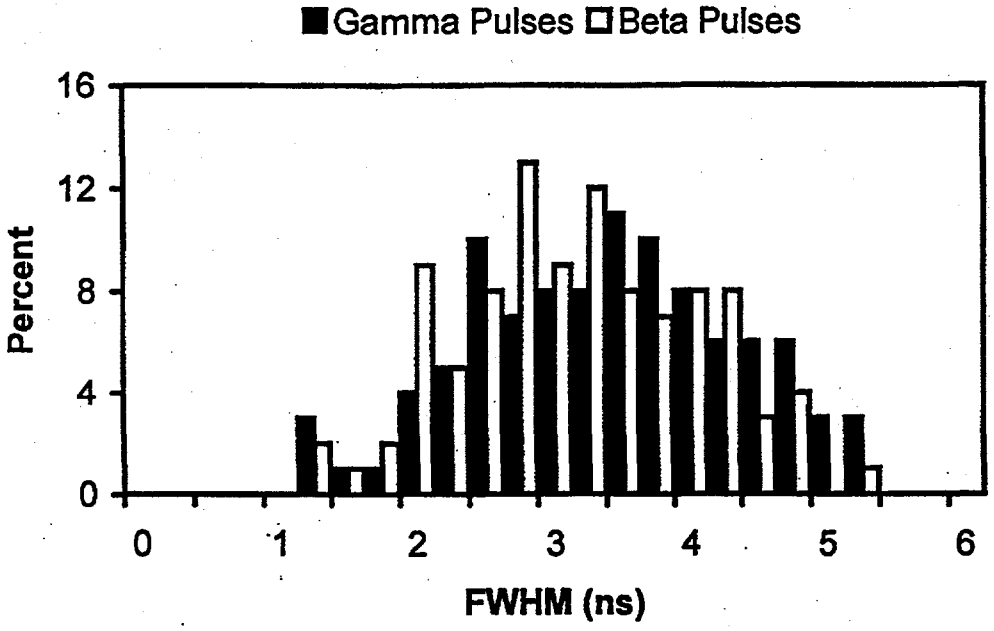

Figure 4.9. Plot Showing Width Spectra for Sets of Pulses Acquired Using Beta and Gamma Radiation, Respectively

5.0 Implementation

We remain optimistic that the unwanted structure described and investigated above will eventually be either eliminated or overcome. In anticipation of this event, we have considered methods for the electronic implementation of DFND as a fieldable system. This section briefly describes the expected implementation.

Although a fast digital oscilloscope and software analysis is used for the laboratory experiments , this method is quite unsuitable for fieldwork. Even if the cost, size, and weight of the scope were not a problem, its limited pulse processing rate would render the system all but useless under realistic conditions. The oscilloscope is only able to pass roughly 10 pulses per second out to a computer for analysis. We estimate that some method must be found to process pulses at a rate of roughly 100 kHz to operate a neutron detector for many applications. (Assuming that 1000 gamma rays are detected for every neutron, this would allow a neutron detection rate of 100 neutrons per second.) Assuming that the electronics eventually have a low replication cost, higher processing rates could be obtained by subdividing the neutron detection system. (Additional information about the detected neutron could also be obtained in this way.)

Figure 5.1 shows a block diagram of the anticipated electronics system. Fast digitizers record the pulses directly from the PMTs, or possibly from fast amplifiers that boost the signal amplitude. We do not yet know for certain how many fast digitizers will ultimately be necessary to record the data at sufficient rates. It is hoped that two "staggered" digitizers running at 1.0 GHz will suffice. A field programmable gate array (FPGA) controls the digitizers and performs a rapid, "rough cut" discrimination between neutron and gamma ray pulses. This initial rough discrimination is not intended to identify neutrons, but rather to identify the large number of obvious gamma ray pulses that can be safely removed from the data stream. Those pulses that are found to be neutron "candidates" are passed by the FPGA to a computer that performs the final analysis and discrimination with software. It is possible that a hardware neural net will be used to implement the rough discrimination; such devices are commercially available.

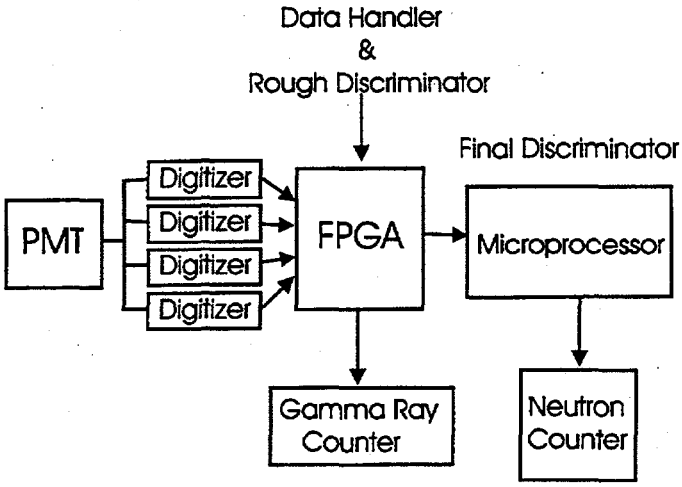

Figure 5.1. Schematic Representation of the Proposed Electronic Implementation of a DFND System

6.0 Next Steps

A number of additional tests are planned that will enable us to bring DFND closer to the point of becoming a viable method for neutron detection. These tests are listed below:

6.1 PMT Testing

It has been suggested that the pulse distortion may arise within the PMT as a result of gain and voltage shifts during the pulse itself. This hypothesis appears to be reasonable, and a multitude of tests are planned to confirm, and then correct this problem.

6.2 Single Photon Tests

Much of the data that is discussed in the academic and product literature on fast plastic scintillators utilizes a test called the "single photon test." This test operates as shown in Figure 6.1. Two distinct PMTs view a particular scintillator. The first PMT is used to accurately time the initiation of an interaction event within the scintillator. The second PMT views the same scintillator through a narrow hole in an absorbing sheet so that only a single photoelectron is likely to be recorded by the PMT. A histogram of the delay time between the interaction event and the arrival of the single photon effectively describes the response of the scintillator.

Previous single photon studies have repeatedly found the response of the scintillator to be very rapid and unstructured (Moszynski and Bengtson 1977; Moszynski and Bengtson1979). Simply put, our results are in sharp disagreement with previous results based on the single photon tests. The difference between these two measurement methods is currently unknown, but may in fact result from the differing uses of the PMT. Before speculation continues along these lines, we intend to reproduce the literature results using our scintillator, thereby ruling out the possibility that modern scintillators have somehow changed since the previous measurements were made. (A possibility that surprisingly cannot be immediately dismissed.)

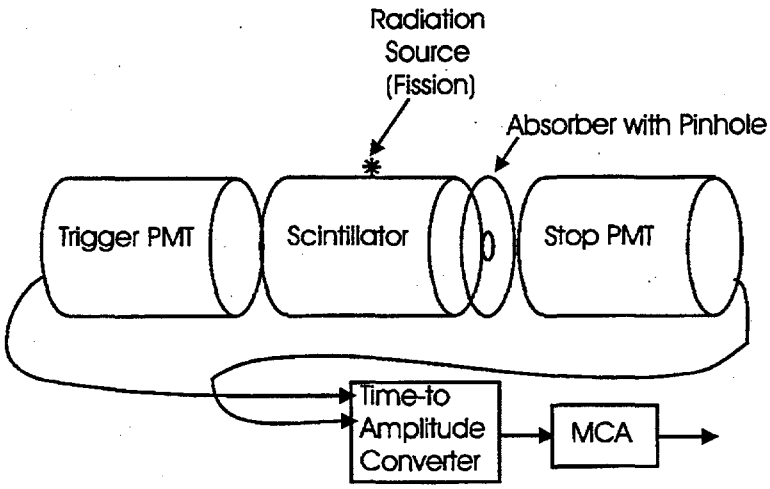

Figure 6.1. Schematic Diagram Showing the Technique Used To Acquire "Single Photon Test" Data

6.3 Low Density Scintillator

An alternate approach to the construction of a successful direct fast-neutron detector is possible even should the unwanted pulse distortion remain. A low-density scintillator should yield gamma ray pulses similar to those currently observed. However, the neutron pulses will be stretched in time and easier to recognize since the neutron recoil timing scales as the inverse of the scintillator density. A scintillator with reduced overall density can be constructed using sheets or rods of scintillator separated by air gaps (Albergo et al. 1995). We might attempt to build such a system to validate the physics behind DFND. This approach may ultimately even offer the best method for construction of a fieldable system.

7.0 References

Albergo S et al. 1995. "Light Pulses To Photomultiplier Tubes From Extended Scintillators," *Nucl. Instrum. And Meth., A* **362**, 423.

Briesmeister J (Editor). 1993. *MCNP -- A General Monte Carlo Code N-Particle Transport Code,* Version 4A, LA-12625-M, Los Alamos National Laboratory, Los Alamos, New Mexico.

Curie I and F Joloit. 1932. "Émission de protons de gran vitesse par les substances hydrogénées sous l'influence des rayons y très pénétrants," *Cont. Rend.* **194** 273.

Heltsley J et al. 1988. "Particle identification via pulse-shape discrimination with a charge-integrating ADC," *Nucl. Instrum. Meth., A* **263** 441.

Knoll GF. 1989. *Radiation Detection and Measurement,* John Wiley & Sons, Inc., New York.

Kunze V, W-D Schmidt-Ott, U Bosch-Wicke, R Böttger, and H Klein. 1995. A Modular 4-Pi Counter For Beta-Delayed Neutrons," *Nucl. Instrum. Meth., A* **361** 263.

Marion JB and FC Young. 1968. *Nuclear Reaction Analysis,* North-Holland, Amsterdam.

Moszynski M and B Bengtson. 1977. "Light pulse shapes from plastic scintillators," *Nucl. Instrum. Meth. A* **142** 417.

Moszynski M and B Bengtson. 1979. "Status of timing with plastic scintillation detectors," *Nucl. Instrum. Meth. A* **158** 1.

Moszynski M et al. 1992. "Study Of N-Gamma Discrimination By Digital Charge Comparison Method For A Large Volume Liquid Scintillator," *Nucl. Instrum. Meth.* A **317** 262.

West RN. 1973. "Positron studies of condensed matter," *Adv. Phys.* **22** 263.

Distribution

No. of
Copies

OFFSITE

2 DOE Office of Scientific and Technical Communications

ONSITE

Pacific Northwest National Laboratory

R. J. Arthur		P8-08
R. A. Craig		K5-25
G. B. Dudder	(5)	K6-48
R. R. Hansen	(5)	P8-20
W. K. Hensley		P8-08
C. W. Hubbard		P8-48
P. E. Keller		K7-22
A.J. Peurrung	(10)	P8-08
P. L. Reeder	(5)	P8-08
D. E. Robertson		P8-20
D. S. Sunberg		P8-08
R. A. Warner		K6-48
Technical Report Files	(5)	